MODELLING OF COMPRESSIBLE FLUID FLOW OF BINARY GAS MIXTURES IN ACOUSTIC RESONANCE SYSTEMS USING OPENFOAM

Conference Paper · May 2021

DOI: 10.1615/TFEC2021.cmd.036663

CITATIONS
0

READS
51

4 authors, including:

Jose Lorenzo Alejandro Barba
University of Leeds
2 PUBLICATIONS **1** CITATION
SEE PROFILE

Xiaoan Mao
University of Leeds
56 PUBLICATIONS **853** CITATIONS
SEE PROFILE

Zinedine Khatir
Birmingham City University
40 PUBLICATIONS **344** CITATIONS
SEE PROFILE

ASTFE
American Society
of Thermal and Fluids Engineers

5th -6th Thermal and Fluids Engineering Conference (TFEC)
May 26-28, 2021
Virtual Conference

TFEC-2021-36663

MODELLING OF COMPRESSIBLE FLUID FLOW OF BINARY GAS MIXTURES IN ACOUSTIC RESONANCE SYSTEMS USING OPENFOAM

José L. A. Barba-Piña,[1,*] Xiaoan Mao,[1] Alan D. Burns,[1] Zinedine Khatir[2]

[1]Faculty of Engineering and Physical Sciences, University of Leeds, LS2 9JT, United Kingdom
[2]Faculty of Computing, Engineering and the Built Environment, Birmingham City University, B5 5JU, United Kingdom

ABSTRACT

In this work, the oscillatory flow of a homogeneous binary gas mixture was simulated in a computational domain consisting of a quarter-wavelength standing-wave acoustic resonator. The set of flow governing equations are the unsteady compressible Navier-Stokes equation, the unsteady continuity equation, the unsteady energy equation, and the state equation for ideal gases. Thermophysical properties of a Ar-Xe mixture were considered for the calculations of viscous and thermal acoustic attenuation effects in the boundary layer region. Simulations were carried out with the open-source CFD package OpenFOAM, using its standard solver for compressible unsteady flow *rhoPimpleFoam*. The standing-wave oscillatory flow was achieved by the implementation of a time-dependent sinusoidal pressure boundary condition, acting as the resonator's acoustic source. Simulation results have shown that pressure and velocity field values are in good agreement with the analytical approximations for an acoustic quarter wavelength resonance channel. Additionally, thermal effects on the boundary layer region are explained by analyzing the heat transfer process occurring within a whole acoustic cycle. This model methodology demonstrates that CFD analysis of flow and heat transport processes in acoustic systems can be used as a predictive tool of the performance of devices where thermal effects are important, and gas mixtures are generally used as the working fluid.

KEY WORDS: Acoustic resonance, Homogeneous gas mixtures, Heat transfer, Compressible flow, CFD, OpenFOAM

1. INTRODUCTION

Numerical modeling of acoustic and thermoacoustic flow problems has demonstrated to be an excellent tool for the analysis of the complex interactions between heat and momentum transport caused by the pressure and flow displacement oscillations [4, 5, 7, 8, 18]. Furthermore, linear mathematical approximations are not enough to explain the nonlinear behavior of the oscillating flow variables present in the majority of real acoustic interactions such as shockwaves and harmonics [9, 11, 14]. In the case of acoustic resonators, the existence of several parameters, such as geometry dependence on the thermophysical properties of the working fluid or the viscous and thermal interactions within the fluid boundary layer represents a constraint for the achievement of optimal resonance conditions [14]. This kind of setbacks found in the experimental work of acoustic devices can be overcome by applying accurate numerical simulation techniques that can help to present a preliminary analysis of the system behavior. Additionally, visualization of characteristic flow variables offered by CFD can be used as a helpful feature for the qualitative description of acoustical flow processes.

*Corresponding José L. A. Barba-Piña: pmjlab@leeds.ac.uk

The usage of acoustic resonators comprises a wide variety of applications such as noise attenuators for external ventilation systems in buildings [2], suppression systems for acoustic instabilities in combustion chambers [12], fluid-container channels in the design of thermoacoustic engine and refrigerator devices. [3, 14, 18], and even as experimental devices for the thermoacoustic separation process of binary gas mixtures [13, 15]. In the last case, separation of the gas mixture was identified by [15] when discrepancies of the expected resonance frequency of a coupled acoustic resonator were observed when using a He-Xe binary gas mixture as the working fluid. This outcome shows that albeit this mass transfer process can affect the performance of acoustic resonance devices, the effect of acoustic oscillations on temperature and velocity gradients can be used for the separation gas mixtures.

The present study is the first step for developing a numerical model for acoustic resonator systems working with gas mixtures, where mass transfer effects caused by molecular thermophoresis and acoustic displacement occur, producing a separation of the gas mixture [15]. For this purpose, it is important to understand the thermal and viscous attenuation effects of the acoustic oscillations occuring in the boundary layer, as the combined effect of temperature and velocity gradients in this region are the main contributors to the mass flux separaion of the mixture.

2. NUMERICAL METHOD

2.1 System Geometry and Computational Domain

Figure 1 shows a hypothetical quarter wavelength acoustic resonator and its computational domain which is used for the simulation work. There are some advantages in the choice of a quarter wavelength cylindrical resonator channel. The first one is the geometrical simplicity offered by the symmetry of a circular channel that allows for reducing the computational domain to half of the original size. Another reason for this choice is that since a quarter wavelength resonator is half of the size of a half-wavelength resonator, the obtention of a converged solution just requires half of the computational domain for the same conditions, this reduction of the effective area of the resonator channel causes a reduction of the thermal losses compared with a half-wavelength resonator which is a desired feature for the operation of thermoacoustic refrigerators [3, 16].

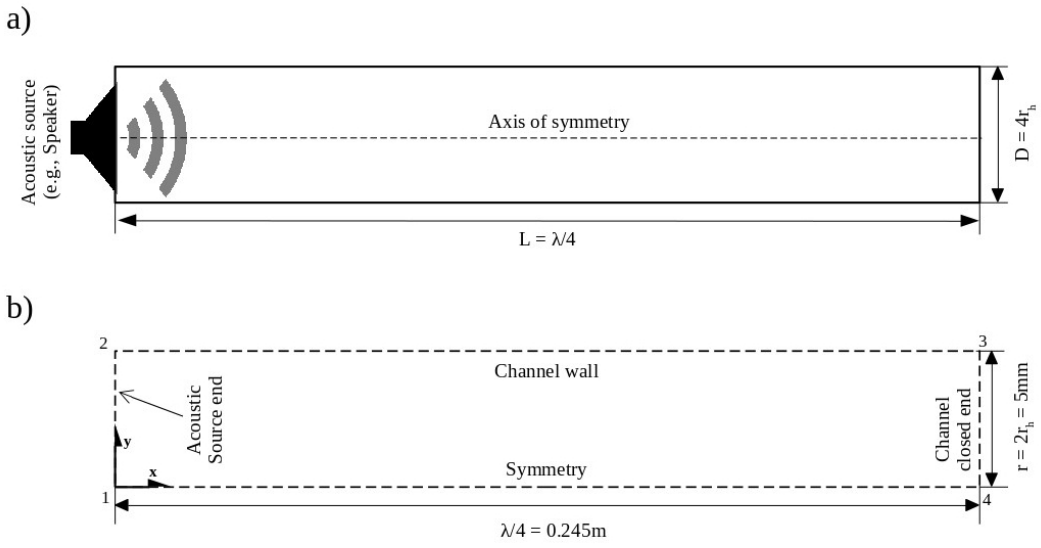

Fig. 1 a) Representation of an acoustic quarter wavelength resonator. b) Quarter wavelength resonator's computational domain and boundary conditions.

2.2 Governing Equations and Boundary Conditions

The system of equations for representing the model consists of the momentum, continuity, and heat transport equations for a compressible laminar flow, with the addition of the ideal-gas equation of state. These equations are written below consecutively, for a two-dimensional cartesian system.

$$\frac{\partial \rho}{\partial t} + \nabla \cdot (\rho \mathbf{v}) = 0 \tag{1}$$

$$\frac{\partial \rho u}{\partial t} + \mathbf{v} \cdot \nabla(\rho u) = -\frac{\partial p}{\partial x} + \nabla \cdot (\mu \nabla u) + S_{Mx} \tag{2}$$

$$\frac{\partial \rho v}{\partial t} + \mathbf{v} \cdot \nabla(\rho v) = -\frac{\partial p}{\partial y} + \nabla \cdot (\mu \nabla v) + S_{My} \tag{3}$$

$$\frac{\partial \rho h_0}{\partial t} + \mathbf{v} \cdot \nabla(\rho h_0) = -\frac{\partial p}{\partial t} + \nabla \cdot (\kappa \nabla T) + S_h \tag{4}$$

$$p = \rho R T \tag{5}$$

Where $h_0 = h + \frac{1}{2}(u^2 + v^2)$ is the total enthalpy of the gas mixture and $h = Cp(T - T_m)$ [4, 10].

Figure 1.b) shows the set of boundary conditions used for the simulation case. according to figure 1, the boundary 1-2 represents the acoustic source of the resonator's. Here, the pressure boundary condition is a simple harmonic oscillator function that works as the acoustic input at the *open end* of a quarter-wavelength resonator, [2, 10, 16]

$$p = p_m + p_A(x) cos(\omega t) \tag{6}$$

The first *RHS* term is the resonator's mean pressure p_m, and the second term is the oscillatory pressure that depends on time and the wave propagation direction $p_1 = p_A(x) cos(\omega t)$ [14]. Additionally, the velocity and temperature boundary conditions at the boundary 1-2 are set as *zero-gradient* condition

$$\nabla u = \nabla v = \nabla T = 0 \tag{7}$$

Then, boundary 2-3 represents the channel wall where the boundary conditions are set as *zero-gradient* for the pressure, a non-slip condition for the velocity vector, and a constant temperature value at the wall assuming that the solid wall has a high enough heat capacity and thermal conductivity to enforce the temperature oscillations to $T_1 = 0$ [14].

$$\nabla p = 0 \tag{8}$$

$$\mathbf{v} = (0, 0, 0) \tag{9}$$

$$T = 300K \tag{10}$$

The boundary 3-4 represents the closed end of the resonance channel, here the boundary conditions are *zero-gradient* for pressure and temperature variables, and velocity vector value is zet to zero as this condition makes the pressure wave to be reflected to the opposite direction of the flow [2],

$$\nabla p = \nabla T = 0 \tag{11}$$

$$\mathbf{v} = (0, 0, 0) \tag{12}$$

Finally, the boundary 1-4 represents the axis of symmetry of the cylindrical resonance channel, as a symmetrical acoustic laminar flow is assumed [14].

The selection of the Xe-Ar mixture as the working fluid was made based on its high average molar mass value and the Prandtl number value for the mean temperature which is $Pr = 0.62$, these characteristics enhance the

thermal efficiency of the gas heat transfer [1] and decreases the value of the sound speed which reduces the wavelength value as well [14]. Since the maximum amplitude of the pressure oscillations is approximately 1% of the mean pressure, the magnitude of temperature oscillations is small enough to consider that a variation in the transport properties values can be ignored. [6] offers a complete database of the transport properties of noble gas binary mixtures which includes the Ar-Xe mixture properties for the simulation work presented in table 1.

2.3 Numerical Algorithm

The solution of the governing equations was carried out with the OpenFOAM solver *rhoPimpleFoam*, this solver is based on the PIMPLE algorithm for undertaking transient calculations of the compressible momentum, continuity, and heat transport equations. [4] offers a detailed explanation of the functionality of this solver for acoustic and thermoacoustic flow applications. Since the *peak* Reynolds number value is $|\overline{Re}| \approx 252$, and the ratio of the resonator's diameter with the viscous penetration depth is $\frac{D}{\delta_\nu} \approx 10$, the flow regime is considered to be at the limit of the laminar and weakly turbulent region according to the oscillatory flow regimes diagram presented in [14]. Thus, the simulation is carried out for the laminar regime since the weak turbulence at the center of the channel does not affect significantly the boundary layer region [14]. The *peak* Reynolds number and the viscous penetration depth are calculated with the following formulas respectively,

$$|\overline{Re}| = \frac{|u_1| D \rho_m}{\mu} \tag{13}$$

$$\delta_\nu = \sqrt{\frac{2\mu}{\omega \rho_m}} \tag{14}$$

For the discretization of time-derivative terms, a hybrid Crank Nicholson-Euler scheme was implemented, while the divergence and laplacian terms discretization was carried out with the QUICK scheme for the velocity vector and the Gauss linear scheme for the scalar fields. Finally, the Gauss linear scheme was used for the discretization of the gradient terms.

The calculation of the discretized equations was carried out with *the generalized geometric-algebraic multi-grid GAMG* solver for the pressure, the *Stabilised preconditioned bi-conjugate gradient for symmetric and asymmetric matrices* for the velocity vector and the *symmetric Gauss-Siedel smooth solver* for the energy and density terms.

Table 1 Mixture thermophysical Properties and Simulation Parameters

n_{Ar}	0.25	f	200 Hz
n_{Xe}	0.75	ω	1256.64 rad/s
$\overline{M}$	0.1085 kg/mol	λ	0.98 m
γ_{mix}	1.667	$\frac{\lambda}{4}$	0.245 m
Cp	191.65 J/(kg K)	r_h	$2.5x10^{-4}$ m
μ	$2.355x10^{-5}\ Pa \cdot s$	δ_ν	$9.223x10^{-5}$ m
κ	$7.32x10^{-3}$ W/(mK)	a	195.8 m/s
Pr	0.62	Δt	$1.25x10^{-5}$ s
p_m	101325 Pa	$max(C)$	0.1
p_A	500 Pa		
T_m	300 K		
ρ_m	4.406 Kg/m^3		
R	75.355 J/KgK		

Table 1 contains the initial conditions and the simulation parameters for the present case. All the thermophysical properties correspond to a homogeneous binary gas mixture with Ar and Xe as its components. The

time-step value is small enough for limiting the maximum value of the Courant number to approximately $C \approx 0.1$ to obtain an independent solution of the time-step size.

Finally, the simulation was stopped after 10,000 time-step iterations, which is equivalent to 0.125 seconds of process time, this is enough for stabilizing the solution field variables, achieving a *pseudo-steady-state* flow condition.

3. RESULTS AND DISCUSSION

3.1 Mesh Sensitivity Analysis

The dependence of the numerical solution with the density of the mesh was analyzed by setting up four simulation cases with four different grid sizes but maintaining the same thermophysical and simulation parameters each time. While the spatial distribution of the cells along the x-direction is uniform for the four grids, the distance between cell elements along the y-direction was gradually reduced within the viscous penetration depth δ_ν for assuring enough resolution inside the boundary layer region.

Table 2 Mesh density refinement with cell elements number

Mesh density	**Cells**
M_1, Coarse	1960
M_2, Medium	8820
M_3, Fine	19600
M_4, Finer	34300

Although the variation of the velocity seems to be very small when the results of the four cases are compared, and all the velocity profiles are equivalent while getting close to the channel wall region due to the extra refinement provided for capturing the boundary layer thermal and viscous effects, it is clear that the solution is practically the same for M_3 and M_4 meshes, as it can be seen in the two plots presented in figure 2. So that, the solution is considered to be independent for a mesh of an approximated size of 19,000 elements like the M_3 case.

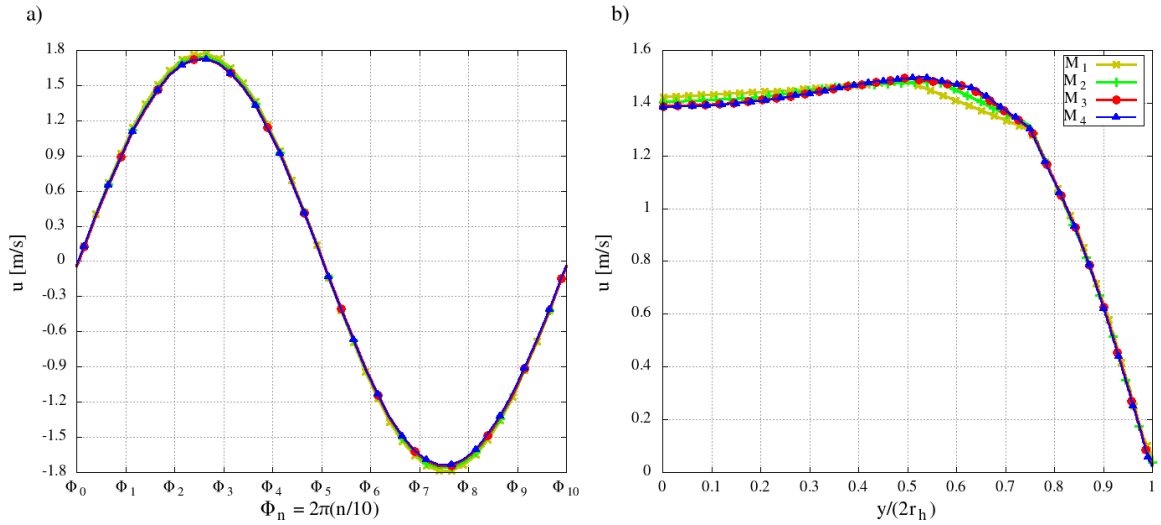

Fig. 2 Mesh sensitivity using the velocity variation as the refinement parameter: a) Velocity distribution at the resonator's central point during a cycle. b) Maximum velocity profiles along y-direction at the center of the resonator.

3.2 Verification of the Model: Simulation Velocity Profiles vs. Analytical Approximation

The verification of the model was made by comparison of the simulation results for the x-component velocity profiles at the center of the resonator with the analytical solution of the thermoacoustic approximation of the momentum equation [14],

$$u = Im[u_1(x, y, z)e^{i\omega t}] \tag{15}$$

$$u_1 = \frac{i}{\omega \rho_m} \left[1 - h_\nu(y, z)\right] \frac{dp_1}{dx} \tag{16}$$

$$h_\nu(z, y) = \frac{J_0\left[(i-1)y/\delta_\nu\right]}{J_0\left[(i-1)2r_h/\delta_\nu\right]} \tag{17}$$

Equation 15 represents the *imaginary* part of the first-order approximation time-dependent term of the oscillating velocity, equation 16 represents a position-dependent velocity x-component function that is a solution of the first-order acoustic approximation of the momentum equation, and equation 17, h_ν represents a complex function that depends on the channel's geometry, being, in this case, the function for a circular thin channel where $\lambda/4 >> D$[11, 14].

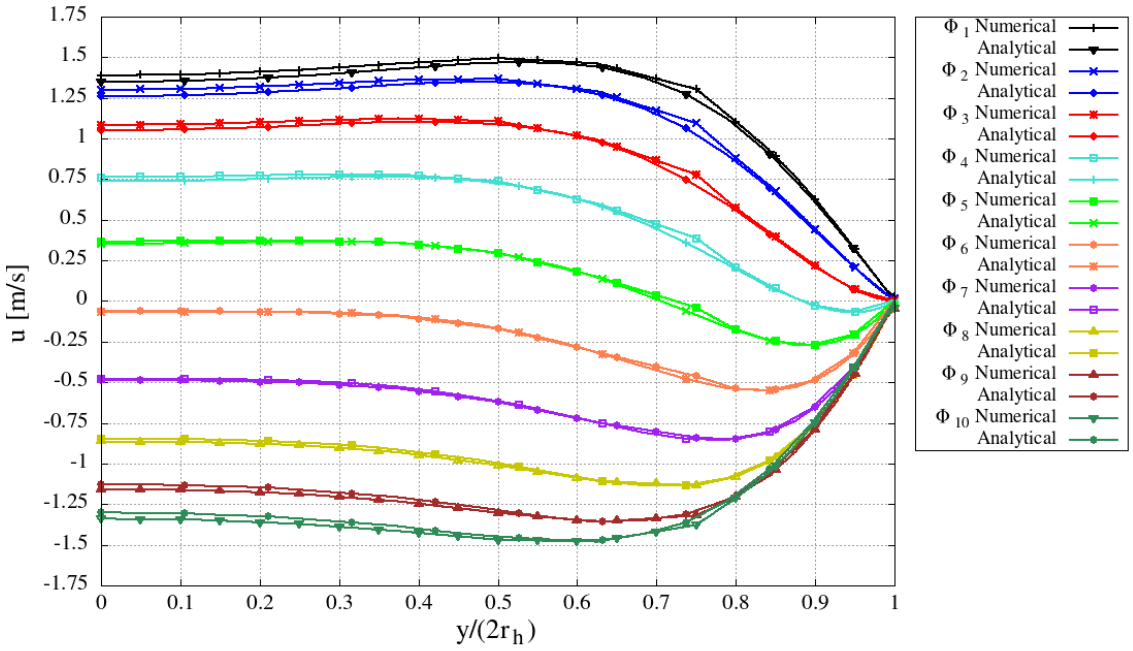

Fig. 3 Comparisson between numerical and analytical velocity profiles along y direction for half of a cycle with $\Phi_n = 2\pi\frac{n}{20}$.

Figure 3 shows the numerical and analytical x-component velocity profiles along half of the cycle. It can be seen that the profiles of both numerical and analytical velocities follow the same pattern, and a slight difference between the values is present. This comparison has been quantified by calculating the relative error of the numerical averaged velocity against the analytical averaged velocity at Φ_1 which is approximately 4.68%.

3.3 Distribution of Flow Variables Along the Resonator's Central Axis

Figure 4 shows the phasing between pressure and velocity over a whole cycle. It can be observed that the pressure leads the velocity by $\frac{2\pi}{5}$ rad. This means that the phasing is close to the acoustic resonance, where the leading variable should be $\frac{\pi}{2}$ rad out of phase [14]. This is a consequence of the pressure and velocity boundary conditions choice, as the resonator's left-end does not represent the exact position of the pressure node due to the small sinusoidal perturbation term that is applied at this point for obtaining a standing wave phasing in a quarter wavelength resonator, and velocity is extrapolated from the internal field velocity value as a consequence of the *zero-gradient* condition [2, 10].

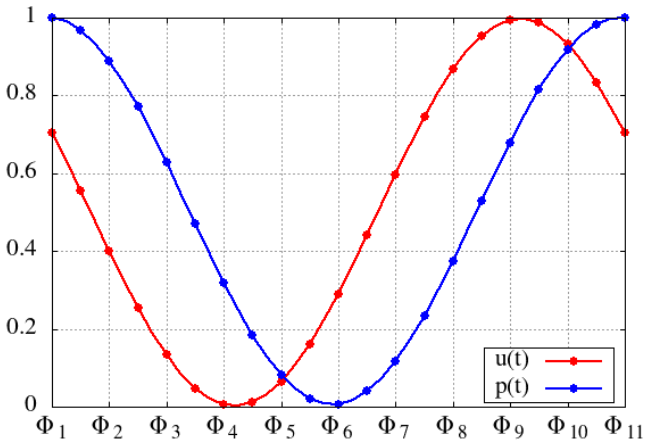

Fig. 4 Phase diagram of the time dependence of pressure and velocity at the center of the resonator with $\Phi_n = 2\pi\frac{n}{10}$.

Figure 5 presents a set of 5 plots of the pressure, velocity and temperature perturbations at different positions of the resonator. Temperature and pressure plots vertical axis represents the first order time-dependent term of the pressure and temperature fields, while the velocity x-component is represented as the imaginary part of the first order time-dependent velocity term [14],

$$p = p_m + Re[p_1 e^{i\omega t}] \tag{18}$$

$$T = T_m + Re[T_1 e^{i\omega t}] \tag{19}$$

$$u = Im[u_1 e^{i\omega t}] \tag{20}$$

From figures 5.a) and 5.c) it is clear that the temperature oscillations along the central axis of the resonator are in phase with the oscillating pressure, which is an expected result due to the direct linear dependence of the temperature with the pressure by the ideal gas equation of state. On the other hand, the temperature profiles on figure 5.e) show how the temperature decreases while approaching the resonator's wall. This is the expected adiabatic behavior of the compression-rarefaction oscillatory process near the resonator's center, and the thermal relaxation at the wall imposed by the constant temperature boundary condition. It is also interesting to observe how the temperature is out of phase with respect to the velocity profiles shown in figure 5.d) this is an important remark which is helpful for explaining the thermoacoustic separation mechanisms of a binary gas mixture in the boundary layer as the combined effects of, temperature gradients, thermodiffusion and velocity gradients in the boundary layer region [13, 15].

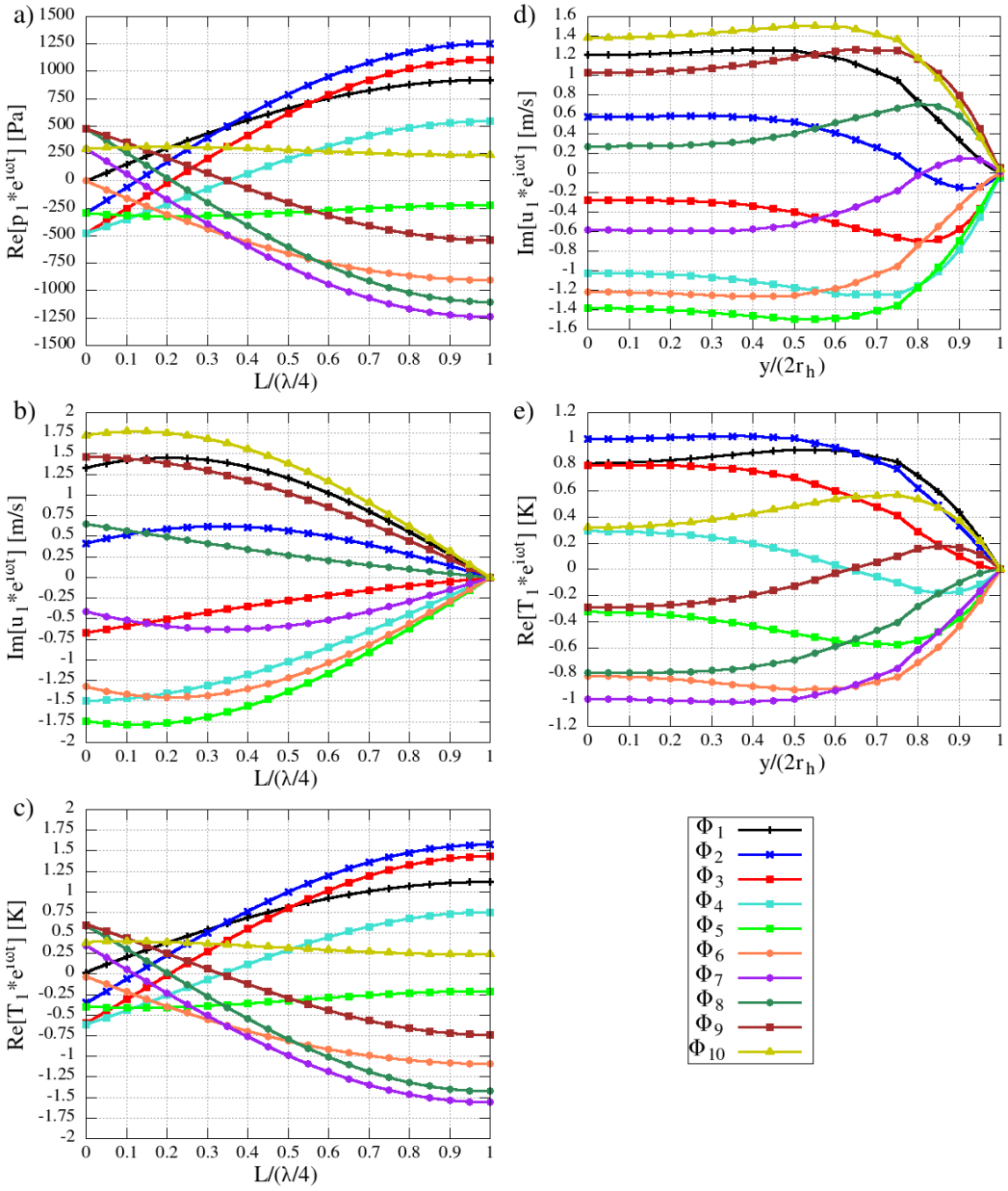

Fig. 5 a) Pressure distribution along the resonator's central x-axis for a whole cycle. b) Velocity x-component distribution along the resonator's central x-axis for a whole cycle. c) Temperature distribution along the resonator's central x-axis for a whole cycle. d) Velocity x-component distribution along the resonator's center y-direction for a whole cycle. e) Temperature distribution along the resonator's center y-direction for a whole cycle.

4. CONCLUSIONS

The simulation of a quarter wavelength acoustic resonator with a binary mixture of Xe-Ar was carried out with the opensource package OpenFOAM, obtaining accurate results of the standing-wave acoustic flow phasing for a quarter-wavelength resonator. Verification of the numerical model against the mathematical approximation suggests that the acoustic flow variables behave as expected by the thermoacoustic theory, with an acceptable relative error value. The small discrepancies can be attributed to the implementation of the pressure boundary condition without considering the displacement of the open-end boundary [17].

Since the assumption of a homogeneous mixture is a simplification of the behavior of a gas mixture under the influence of an acoustic field, rejecting the mass transfer occurring within the boundary layer, future work will be focused on obtaining a model capable of capturing the mass transfer process of the separation of the gas mixture due to temperature and velocity gradients within the boundary layer region as presented by [15]. Also, it will be necessary to test larger pressure amplitude values and different geometrical and thermophysical initial conditions in order to identify the reach and limitations of the present model.

ACKNOWLEDGMENTS

The authors acknowledge Mexico's National Council of Science and Technology (CONACyT) and Energy Secretariat (SENER) for providing the funds for José Lorenzo A. Barba-Piña's Ph.D. studies at the University of Leeds (Reference No. 625883 / 472622). This work was undertaken on ARC4, part of the High-Performance Computing facilities at the University of Leeds, UK.

NOMENCLATURE

ρ_m	Mean gas density	(kg/m^3)	L	Channel length	(m)
Φ	Phase angle	(rad)	r_h	Hydraulic radius	(m)
λ	Wavelength	(m)	D	Channel diamter	(m)
μ	Dynamic viscosity	(Pa.s)	f	Frequency	(Hz)
κ	Thermal conductivity	(W/mK)	T	Oscillation period	(s)
ω	Angular frequency	(rad/s)	a	Speed of sound	(m/s)
δ_ν	Viscous penetration depth	(m)	p_m	Mean Pressure	(Pa)
γ	specific heats ratio	(-)	p_A	Pressure amplitude	(Pa)
J_0	First kind Bessel function of order 0	(-)	p_1	Oscillatory pressure, 1^{st} order term	(Pa)
Pr	Prandtl number	(-)	r_h	Hydraulic radius	(m)
$\lvert\overline{R}e\rvert$	Peak Reynolds number	(-)	T_m	Mean temperature	(K)
C	Courant number	(-)	T_1	Oscillatory temperature, 1^{st} order term	(K)
n_a	Mole fraction of specie a	(-)	$\mathbf{v}$	Velocity vector	(m/s)
h_0	Total enthalpy	(J)	u, v, w	Velocity vector *x,y,z* components	(m/s)
$\overline{M}$	Molar mass	(Kg/mol)	u_1	oscillatory velocity, 1^{st} order term	(m/s)
c_p	Isobaric heat capacity per unit mass	(J/KgK)	Δt	Simulation time step	(s)
$\overline{R}$	Universal gas constant	(J/molK)	$Re[z]$	Real part of the complex z	(-)
R	Specific gas constant	(J/KgK)	$Im[z]$	Imaginary part of the complex z	(-)

REFERENCES

[1] Campo, A., Papari, M. M., and Abu-Nada, E., "Estimation of the minimum prandtl number for binary gas mixtures formed with light helium and certain heavier gases: Application to thermoacoustic refrigerators," *Applied Thermal Engineering*, 31(16), pp. 3142–3146, (2011).

[2] Field, C. and Fricke, F., "Theory and applications of quarter-wave resonators: A prelude to their use for attenuating noise entering buildings through ventilation openings," *Applied Acoustics*, 53(1), pp. 117–132, (1998).

[3] Garrett, S. L., Adeff, J. A., and Hofler, T. J., "Thermoacoustic refrigerator for space applications," *Journal of Thermophysics and Heat Transfer*, 7(4), (1993).

[4] Gonzalez, E., "Cfd simulations of acoustic and thermoacoustic phenomena in internal flows," *Proc. of 46th AIAA Fluid Dynamics Conference*, American Institute of Aeronautics and Astronautics, (2016).

[5] Ilori, O., Mao, X., and Jaworski, A., "Numerical simulation of oscillatory flow and heat transfer in the heat exchangers of thermoacoustic systems," *Proc. of 24th IIR International Congress of Refrigeration*, (2015).

[6] Kestin, J., Knierim, K., Mason, E. A., Najafi, B., Ro, S. T., and Waldman, M., "Equilibrium and transport properties of the noble gases and their mixtures at low density," *Journal of Physical and Chemical Reference Data*, 13(1), pp. 229–303, (1984).

[7] Li, B. and You, J. H., "Simulation of acoustic energy harvesting using piezoelectric plates in a quarter-wavelength straight-tube resonator," *Proc.of 2012 COMSOL Conference, Boston*, p. 7, (2012).

[8] Mergen, S., Yıldırım, E., and Turkoglu, H., "Numerical study on effects of computational domain length on flow field in standing wave thermoacoustic couple," *Cryogenics*, 98, pp. 139–147, (2019).

[9] Merkli, P. and Thomann, H., "Thermoacoustic effects in a resonance tube," *Journal of Fluid Mechanics*, 70(1), pp. 161–177, (1975).

[10] Namdar, A., Kianifar, A., and Roohi, E., "Numerical investigation of thermoacoustic refrigerator at weak and large amplitudes considering cooling effect," *Cryogenics*, 67, pp. 36–44, (2015).

[11] Rott, N., "Damped and thermally driven acoustic oscillations in wide and narrow tubes," *Zeitschrift für angewandte Mathematik und Physik ZAMP*, 20(2), pp. 230–243, (1969).

[12] Sohn, C. H. and Park, J. H., "A comparative study on acoustic damping induced by half-wave, quarter-wave, and helmholtz resonators," *Aerospace Science and Technology*, 15(8), pp. 606–614, (2011).

[13] Spoor, P. S. and Swift, G. W., "Thermoacoustic separation of a he-ar mixture," *Physical Review Letters*, 85(8), pp. 1646–1649, (2000).

[14] Swift, G. W., *Thermoacoustics: A Unifying Perspective For Some Engines And Refrigerators*, Springer International Publishing, (2017).

[15] Swift, G. W. and Spoor, P. S., "Thermal diffusion and mixture separation in the acoustic boundary layer," *The Journal of the Acoustical Society of America*, 106(4), pp. 1794–1800, (1999).

[16] Tasnim, S. H. and Fraser, R. A., "Computation of the flow and thermal fields in a thermoacoustic refrigerator," *International Communications in Heat and Mass Transfer*, 37(7), pp. 748–755, (2010).

[17] Tisovsky, T. and Vit, T., "Design of numerical model for thermoacoustic devices using OpenFOAM," *Proc. of 36TH MEETING OF DEPARTMENTS OF FLUID MECHANICS AND THERMODYNAMICS*, AIP Publishing, (2017).

[18] Zink, F., Vipperman, J., and Schaefer, L., "Cfd simulation of thermoacoustic cooling," *International Journal of Heat and Mass Transfer*, 53(19), pp. 3940–3946, (2010).